

High-parallelism Inception-like Spiking Neural Networks for Unsupervised Feature Learning

Mingyuan Meng^{a,b,†}, Xingyu Yang^{a,‡}, Lei Bi^b, Jinman Kim^b, Shanlin Xiao^{a,*}, Zhiyi Yu^{a,*}

^a School of Electronics and Information Technology, Sun Yat-sen University, Guangzhou, China

^b Biomedical & Multimedia Information Technology Research Group, School of Computer Science, The University of Sydney, Sydney, Australia

Abstract: Spiking Neural Network (SNN) is a brain-inspired, event-driven machine learning algorithm that has recognized potential in producing ultra-high-energy-efficient hardware. Among existing SNNs, unsupervised SNNs are based on synaptic plasticity and considered to have more potential in imitating the learning process of biological brain. Most unsupervised SNNs are trained through competitive learning with Spike-Timing-Dependent Plasticity (STDP). However, the STDP-based SNNs are limited by slow learning speed and/or constrained learning capability. In this paper, to overcome these limitations, we: 1) designed a high-parallelism network architecture, inspired by the Inception module in the Artificial Neural Network (ANN) literature; 2) extended a widely used vote-based spike decoding scheme to a Vote-for-All (VFA) decoding layer to reduce the information loss in the spike decoding; 3) proposed to use adaptive repolarization (i.e. resetting) in the spiking neuron model to enhance the spiking activities and thus further accelerate the network's learning. We evaluated our contributions on the two established benchmark datasets (MNIST/EMNIST). Our experimental results show that our architecture exhibits superior performance than widely used Fully-Connected (FC) and Locally-Connected (LC) architectures. Our SNN not only achieves comparable results with the state-of-the-art unsupervised SNNs (95.64%/80.11% accuracy on the MNIST/EMNIST dataset), but also shows superior learning efficiency and robustness against hardware damage. Our SNN trained with only hundreds of iterations can achieve a great classification accuracy, and random destruction of large numbers of synapses and neurons only leads to negligible performance degradation.

Keywords: Spiking Neural Network, Unsupervised Learning, Inception Module, Learning Efficiency, and Robustness.

1 Introduction

Recently, ANN has made good progress in many cognitive tasks (e.g. recognition, analytics, and inference) [19-21]. However, ANN is computational-intensive [16], and thus motivating research on brain-inspired spiking neural network (SNN) to lessen the computation[2]. Unlike the traditional ANN whose neuron is characterized by a single, static, continuous-valued activation, in contrast, the SNN resembles the brain's biological function of its neurons by using discrete spikes to compute and transmit information. SNN is thus arguably the only viable way to understand how the brain computes at the neuronal description level [2]. The power consumption and latency of SNN can be significantly reduced, compared to ANN, due to its event-driven style of computing [16-18].

Most existing SNN learning algorithms can be divided into three categories: *supervised*, *unsupervised*, and *conversion*. *Supervised/Unsupervised* denotes the algorithms of training SNN with/without label information. Specifically, the supervised algorithm uses a loss function to guide the SNN's training which aims at reducing the differences between the actual output and the target output (label) [3-6]. The unsupervised algorithms let the neurons adjust their own synaptic weights based on biological synaptic plasticity and learn the inner structure of the input examples without labels [7-14]. *Conversion* denotes the algorithms of converting a trained ANN into a SNN to circumvent the difficulties in training SNN directly [15-18]. In this paper, we focus on unsupervised SNN because the

This work is supported in part by the grants 2017YFA0206200, 2018YFB2202601 from National Key R&D Program of China, and the grants 61674173, 61834005, and 61902443 from National Nature Science Foundation of China (NSFC).

[†] M. Meng and X. Yang contributed equally to this paper. ^{*} S. Xiao and Z. Yu both are corresponding authors.

E-mail: mengmy3@mail.sysu.edu.cn (M. Meng), yangxy266@mail2.sysu.edu.cn (X. Yang), lei.bi@sydney.edu.au (L. Bi), jinman.kim@sydney.edu.au (J. Kim), xiaoshlin@mail.sysu.edu.cn (S. Xiao), yuzhiyi@mail.sysu.edu.cn (Z. Yu).

unsupervised algorithms based on synaptic plasticity are considered to be more biologically plausible with higher resemblance to the learning process of biological brain [1].

Most unsupervised SNN algorithms train the SNN through competitive learning based on Spike-Timing-Dependent Plasticity (STDP) [7-13]. This STDP-based approach allows the SNN to learn in a fully unsupervised fashion without any label information. Despite this advantage, existing unsupervised SNN algorithms have several limitations: preliminary work by Diehl et al. [7] using a Fully-Connected (FC) network architecture only exhibited sub-optimal learning capability (95.00% accuracy on the MNIST), and it was extremely slow on training (900,000 iterations were needed). Later works focused on more advanced learning rules (e.g. Adaptive Synaptic Plasticity (ASP) [9] and stochastic STDP [10]). These works indeed improved the SNN's learning capability, but they were still limited by the FC architecture, and thus resulting in unsatisfactory learning efficiency. More recently, Locally-Connected (LC) network architecture was used in SNN [8] which improved the learning speed (60,000 iterations were needed) and robustness against hardware damage. Nonetheless, the LC architecture's improvement in learning capability was marginal (95.07% accuracy on the MNIST). In this paper, we followed the research track of LC architecture, and focused on the design of network architecture to propose an unsupervised STDP-based SNN, in order to improve in measures of learning speed, robustness, as well as learning capability.

Learning efficiency and robustness are highly relevant to the architecture's parallelism (discussed in Section 7.1). For improving the architecture's parallelism, the Inception module [22] in the ANN literature is a good motivation. There is a Split-and-Merge strategy in the Inception module: The input is split into a few parallel pathways with multi-scale filters (e.g. 3×3 , 5×5 , 7×7 convolutional kernels, pooling, etc.), and then all pathways are concatenated together. Through this Split-and-Merge architecture, the Inception modules can process multi-scale spatial information and improve the network's parallelism. Inspired by this Split-and-Merge strategy, we designed an Inception-like multi-pathway network architecture (see Fig. 3). To further improve the architecture's parallelism, we divided each pathway into multiple parallel sub-networks by partitioning competition areas (see Section 4.1 for more details).

We also found that the widely used vote-based spike decoding scheme (detailed in Section 3.4) doesn't work with the LC and our architectures. This is due to the underlying assumption of the vote-based decoding scheme being violated. The classic vote-based decoding scheme assumes that each output neuron is only highly responsive to one certain class and builds a Vote-for-One (VFO) relationship between each output neuron to a certain class. However, this assumption is infeasible in the LC and our architecture, which leads to a large information loss in the spike decoding (discussed thoroughly in Section 7.2). Therefore, we extended the classic vote-based spike decoding scheme to a Vote-for-All (VFA) decoding layer to avoid this problem by building a VFA relationship between each output neuron and all possible classes. (see Section 4.2 for more details).

Besides, the learning speed of STDP-based SNN is highly relevant to its spiking intensity, because the update of synaptic weight (i.e. learning) occurs when the pre/postsynaptic neuron fires a spike (discussed thoroughly in Section 7.3). To further accelerate the SNN's learning, we proposed to use adaptive repolarization (i.e. resetting) in the spiking neuron model. This adaptive repolarization can enhance the spiking activities of winner neurons, and thus accelerate the SNN's learning (see Section 4.3 for more details).

To sum up, in this paper we proposed an unsupervised STDP-based SNN including three key contributions:

- We designed a high-parallelism Inception-like network architecture for SNN. This architecture integrates multi-scale spatial information (features) and has high-parallelism, thus exhibiting improved learning capability, learning efficiency, and robustness against hardware damage.
- We extended the widely used vote-based spike decoding scheme to a VFA decoding layer to reduce the information loss in the spike decoding.
- We used adaptive repolarization in the spiking neuron model, which can enhance the spiking intensity to accelerate the SNN's learning.

We demonstrate the improvements in our architecture to the state of the art by evaluating with the well-established hand-written digit/letter classification tasks with two public, well-benchmarked datasets (MNIST [23]/EMNIST [24]).

2 Related Work

Inception module was first proposed in [22] and then evolved to many variants [25-26] in the ANN literature. The earlier instance of Inception with SNN was reported by Xing et al. [15]; however, in this work, its SNN needed to be trained through a network conversion (i.e. from trained ANN to SNN). From our review of the literature, we are the first to incorporate Inception-like architecture into unsupervised SNNs. This proposed research introduces the Inception-like architecture and demonstrates its superior performance compared to widely used FC/LC architectures

with a preprint in [39]. By using [39] as the baseline, we demonstrated that our Inception-like architecture can be extended and used as a multi-layer unsupervised SNN [38].

Diehl et al. [7] is one of the earliest papers to train an unsupervised SNN through STDP-based competitive learning. It used a FC architecture combined with a relatively simple learning rule. This approach is limited by sub-optimal learning capability and extremely slow learning speed. To overcome these limitations: In the aspect of learning rule, Panda et al. [9] proposed an Adaptive Synaptic Plasticity (ASP), inspired by the ‘ability to forget’ in the human brain. She et al. [10] proposed to incorporate stochastic STDP into the network architecture of [7]. These methods indeed improve the SNN’s learning capability, but they are still limited by the slow-learning FC architecture. In the aspect of network architecture, Rathi et al. [11] proposed a STDP-based pruning method to compress the FC architecture into a sparsely connected architecture. Saunders et al. [8] proposed to replace the FC connections in [7] with LC connections and got a LC SNN. These methods improve the SNN’s learning efficiency and robustness against hardware damage, but the improvement they gained on learning capability is marginal. Besides, some works focused on the implementations of unsupervised SNN on the neuromorphic hardware (e.g. Lammie et al. [12]).

Moreover, some works used convolutional SNNs [27-30]. Although these methods achieved higher inference accuracy, their SNNs were only used to extract features, and they required extra supervised classifiers (e.g. SVM, supervised FC layer) to complete the classifications. Therefore, they are often considered as semi-supervised algorithms instead of purely unsupervised algorithms [8].

3 Fundamentals

In this section, we describe the fundamental components of SNN, including spiking neuron model, synapse model, spike coding, and competitive learning implementation. The models/methods described in this section are used in our SNN as default if no extra setting is stated.

3.1 Spiking Neuron Model

Spiking neuron model is the basic computing unit of SNN. For the computing efficiency, Leaky Integrate-and-Fire (LIF) model is widely used due to its simplicity, but there are many more complicated neuron models which implement more biological neuron behaviors (e.g. Hodgkin-Huxley (HH) model [31], Izhikevich model [32], and Spike Response Model (SRM) [33]). Following [7], in this paper, we only use a simple conductance-based LIF model to emphasize the effectiveness of our contributions. Other more advanced spiking neuron models can be considered, but the simple LIF model has worked very well. The dynamics of the used LIF model is given by:

$$\tau_v \frac{dv}{dt} = v_{rest} - v + (v_{exc} - v)g_e + (v_{inh} - v)g_i, \quad (1)$$

$$\tau_{g_e} \frac{dg_e}{dt} = -g_e + \sum_i^{N_{exc}} w_i F(s_i, t) \tau_{g_e}, \quad (2)$$

$$\tau_{g_i} \frac{dg_i}{dt} = -g_i + \sum_i^{N_{inh}} w_i F(s_i, t) \tau_{g_i}. \quad (3)$$

In (1), v is the membrane voltage (membrane potential), v_{rest} is the resting voltage, $g_{e/i}$ denotes the total excitatory/inhibitory conductance that is input to the neuron, $v_{exc/inh}$ is the equilibrium voltage of excitatory/inhibitory conductance, and $\tau_{v/g_e/g_i}$ is the time constant of $v/g_i/g_i$. In (2) and (3), $N_{exc/inh}$ is the number of excitatory/inhibitory synapses connected to the neuron, s_i is a synapse, and w_i is the synaptic weight of s_i . The function $F(s_i, t)$ is equal to 1 when a spike is transmitted by s_i at time t , otherwise it’s equal to 0. According to (1), (2) and (3), the v and $g_{e/i}$ decay exponentially to v_{rest} and 0 respectively when no spike arrives. At the occurrence of a spike from an excitatory/inhibitory synapse, the $g_{e/i}$ increases by the weight of this synapse, thus leading to the increase/decrease of the membrane voltage v . When the v reaches or exceeds a threshold v_{thres} , the neuron fires a spike (i.e. depolarization) to downstream neurons, and the v is reset (i.e. repolarization) to a voltage v_{reset} . After firing a spike, the neuron does not integrate input spikes for a refractory period T_{ref} .

Moreover, a homeostasis mechanism in [7] is adopted to ensure that no neuron can fire excessive spikes and dominate the firing activity. The homeostasis is an adaptive threshold scheme as follows:

$$\tau_\theta \frac{d\theta}{dt} = v_{thres} - \theta + \tau_\theta \theta_{plus} F_n(t), \quad (4)$$

where θ is the adaptive threshold (replacing the original fixed threshold voltage v_{thres}), τ_θ is time constant of θ , and function $F_n(t)$ is equal to 1 when the neuron fires a spike at time t , otherwise it’s equal to 0. According to (4), each time the neuron fires a spike, the threshold θ increases by a constant θ_{plus} , or it decays exponentially to the v_{thres} .

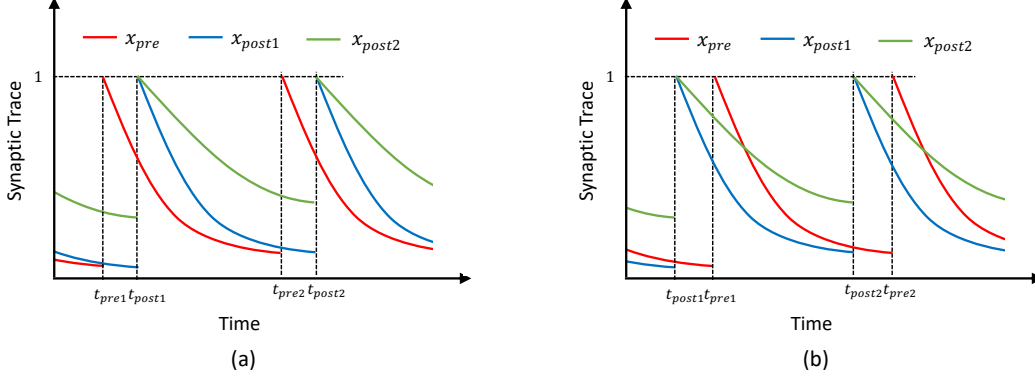


Fig. 1. An illustration of triplet STDP, which shows the behaviors of synaptic traces when (a) presynaptic spikes tend to occur immediately before postsynaptic spikes, and when (b) presynaptic spikes tend to occur immediately after a postsynaptic spike.

3.2 STDP Synapse Model

STDP synapse model was widely used in unsupervised SNNs [7-13] to control the behaviors of synaptic weight. It has evolved to many variants (e.g. additive STDP [34], triplet STDP [35], and stochastic STDP [10]). In this paper, following [7] and [8], we adopt the triplet STDP and simplify it to:

$$\Delta w = \begin{cases} \eta_{post} x_{pre} x_{post2} & \text{when postsynaptic spike} \\ -\eta_{pre} x_{post1} & \text{when presynaptic spike} \end{cases}, \quad (5)$$

where x_{pre} and $x_{post1/post2}$ are presynaptic and postsynaptic traces [36], η_{pre}/η_{post} are the pre/postsynaptic learning rates. The update of synaptic weight w occurs when pre/postsynaptic neuron fires a spike (named pre/postsynaptic spike). The x_{pre} or $x_{post1/post2}$ are reset to 1 when a presynaptic or postsynaptic spike is fired, or they decay exponentially to 0 with $\tau_{pre}/\tau_{post1}/\tau_{post2}$ as the time constant of $x_{pre}/x_{post1}/x_{post2}$. The use of these synaptic traces is actually equivalent to recording the time when the latest pre/postsynaptic spike is fired. Note that we set $\eta_{post} \gg \eta_{pre}$ to emphasize the effects of presynaptic neurons on postsynaptic neurons.

The triplet STDP described in (5) adjusts the synaptic weight based on the relative timing of pre/postsynaptic spikes. Fig.1 is an illustration of triplet STDP model, in which the t_{pre}/t_{post} denotes the time when a pre/postsynaptic spike is fired. As is shown in Fig.1, if presynaptic spikes tend to occur immediately before postsynaptic spikes (Fig.1(a)), the synaptic weight tends to be larger. This is because the x_{post1} has already decayed to a relatively small value when presynaptic spikes trigger the update of synaptic weight w , while the x_{pre} is still a relatively large value when postsynaptic spikes are fired. Similarly, if presynaptic spikes tend to occur immediately after postsynaptic spikes (Fig.1(b)), the synaptic weight tends to be smaller. Competitive learning was proposed mainly based on the former phenomenon (see Section 3.5), which explains why we set $\eta_{post} \gg \eta_{pre}$ to emphasize the former phenomenon. Besides, compared with the typical STDP model, the triplet STDP also considers the time interval of postsynaptic spikes. If the time interval between current and last postsynaptic spikes is too large, the x_{post2} will decay to a very small value, so the synaptic weight w is still hard to increase even though presynaptic spikes occur immediately before postsynaptic spikes.

3.3 Rate-based Input Encoding

Normally, the natural input of many applications is analog value (e.g. image pixel), but SNN expects spikes. Therefore, encoding analog input value into a discrete spike train is needed. In this paper, we adopted a popular rate-based encoding scheme used in [7-13]. The input neuron (i.e. the neurons in the input layer) is a generator of Poisson-distributed spike trains. Each input neuron is responsive to a pixel of the input image. After encoding, each pixel value is represented by a Poisson-distributed spike train, and the average rate of the spike train is determined by the corresponding pixel value multiplied by an encoding parameter λ . Besides, SNN might be insensitive to some training samples, thus leading to low output spiking intensity and slow learning speed. Therefore, we adopted the adaptive encoding scheme used in [7], in which the λ can be adaptive when the SNN's output spiking intensity is too low.

3.4 Vote-based Spike Decoding

Since the output of SNN is spike trains, we need to decode the output spike trains into recognizable classification results when we want to apply a trained SNN on the classification task. In other words, we need to construct a

relationship between the patterns of output spike trains and the classification results. This is the only step where labels are used.

In general, the unsupervised SNNs with rate-based input encoding use vote-based methods for spike decoding [7-13]. A classic vote-based spike decoding scheme was widely used in many unsupervised SNNs [7, 9-13]. In this decoding scheme: First, each output neuron (i.e. the neuron in the output layer) is assigned to a certain class based on its highest spiking response, and a VFO relationship between each output neuron and a certain class is built. Then, during inference, each spike fired by the output neuron is a single vote for its assigned class. Finally, the class having the most votes is the inference result.

The classic vote-based decoding scheme mentioned above works well in most unsupervised SNNs with FC architecture, but we found this scheme doesn't work well in LC architecture and our proposed architecture. Therefore, we proposed a VFA decoding layer to reduce the information loss in the spike decoding. This part will be further discussed in Section 7.2.

3.5 Competitive Learning

Competitive learning was widely used as a training approach in many unsupervised SNNs [7-13]. It's based on the STDP model and its principle is that: we make output neurons compete with each other to learn a certain feature. Each neuron represents a randomly initialized feature at the beginning. Every time a training sample is input, only the winner neuron (i.e. the one whose represented feature is the most similar to the input feature) can fire spikes and adjust its STDP-modifiable (i.e. modified based on STDP) synaptic weights to learn this input feature. Through training, the represented feature of each neuron will become more and more similar to the real input feature. Finally, each neuron will be highly responsive to a certain feature, so they can be used to infer the class of the unseen sample.

The implementations of competitive learning are shown in Fig. 2: The output layer is connected to the input layer with STDP-modifiable synapses. Here we define that the output neurons sharing the same Receptive Field (RF) (i.e. sharing the same set of presynaptic neurons) are in the same competition area. Each output neuron competes with other output neurons in the same competition area. Note that this design is also called lateral inhibition in many works of literature [7, 9, 11-13]. Fig. 2(a) is a preliminary version of competitive learning: The output layer is connected to an inhibitory layer with fixed excitatory synapses in a one-to-one manner. Then, each neuron in the inhibitory layer, using a fixed inhibitory synapse, is connected to all output neurons located in the same competition area except for the one it receives connection from. Besides, there is an alternative version in Fig. 2(b): The inhibitory layer is replaced by the inter-connections between output neurons. Each output neuron is directly connected to other output neurons in the same competition area with fixed inhibitory synapses. The alternative version requires less spiking neurons than the preliminary version, so it's used in this paper as default.

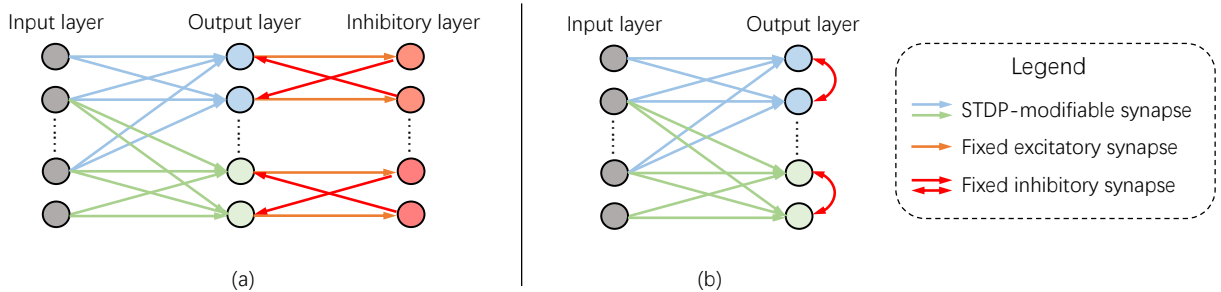


Fig. 2. The implementations of competitive learning. (a) Preliminary version: An inhibitory layer is used to conduct competitions among output neurons. (b) Alternative version: The inhibitory layer is removed, and the output neurons are directly interconnected with fixed inhibitory synapses. Note that the output neurons in the same competition area are drawn in the same color.

4 Method

4.1 High-Parallelism Network Architecture

Fig. 3 is an illustration of our proposed network architecture. Inspired by the Inception module in the ANN literature, we designed a high-parallelism architecture. There are three independent pathways where an output layer is connected to the input layer in a FC/LC manner. The three pathways can compute in parallel without any interaction. A VFA decoding layer is connected to the three output layers in a FC manner to integrate information from the three pathways, and then decode the output spike trains into a recognizable inference result.

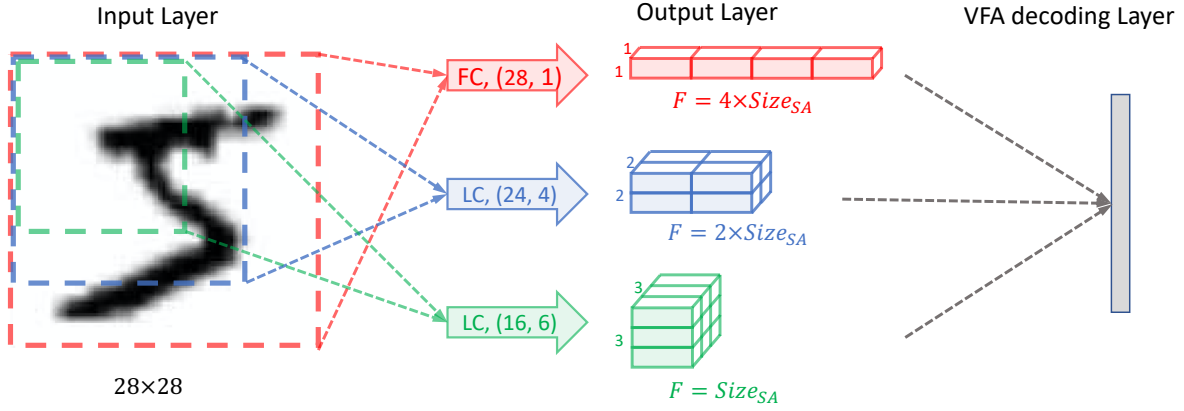


Fig. 3. An illustration of our proposed high-parallelism network architecture. There are three parallel pathways connected to the input layer, each of which has different RF and network topology to cope with image features at different scales. The multi-scale information is finally integrated by a VFA decoding layer. Note that each cube in the output layer denotes a parallel competition area or sub-area.

The neuron in the input layer is the spike train generator described in Section 3.3, and the neuron in the output layer is the conductance-based LIF model described in Section 3.1. Following the principle of competitive learning described in Fig. 2(b), the output layers are connected to the input layer with the excitatory STDP-modified synapses, and the output neurons in the same competition area (i.e. sharing the same RF) are interconnected with the fixed inhibitory synapses.

The LC connection between the output and input layer has the same topology with the convolutional connection but doesn't share weights. Because only square kernel is used in this paper, we only use one kernel size parameter k and one stride parameter s to define the RF (denoted by (k, s) in Fig. 3), and use a F to denote feature map number. Note that the FC connection actually is a special case of the LC connection where the kernel size is equal to the input layer size. So, we also use k , s , and F to define a FC connection with (28,1) as its (k, s) . In this case, each output neuron in the FC connection can be regarded as a feature map. The topology of each pathway is shown in Fig. 3: The RF size of each pathway is different, which means each pathway can cope with the image features at different scales. The multi-scale features finally merge together in the VFA decoding layer.

Moreover, to further improve the architecture's parallelism, we partition the original competition area into several sub-areas, and only allow the output neurons in the same sub-area to conduct competitions. More specifically, as is shown in Fig. 3, the only competition area in the 1st output layer is partitioned into 4 sub-areas, the 4 competition areas in the 2nd output layer are partitioned into 8 sub-areas, while the 9 competition areas in the 3rd output layer remain unchanged. Finally, we manually set each output layer's F to make sure all sub-areas are equal in size. If we define a parameter Size_{SA} as the size of sub-area, the F of the 1st/2nd/3rd output layer should be $4\text{Size}_{SA}/2\text{Size}_{SA}/\text{Size}_{SA}$. After this partitioning, our architecture has 21 individual competition areas, which is equivalent to 21 parallel sub-networks. This part will be further discussed in Section 7.1.

Note that the design of our architecture is highly empirical. Other design can be considered if only it meets the following principles: 1) There are multiple independent pathways, each of which has different RF size to cope with the image features at different scales; 2) The original competition area can be partitioned into sub-areas, but all sub-areas should be equal in size. This part will be further discussed in Section 7.1.

4.2 VFA Decoding Layer

The *Vote-for-all* (VFA) means each output neuron needs to vote for all classes, so the VFA decoding layer is connected to three pathways in a FC manner to receive the votes from all output neurons. This decoding layer can integrate multi-scale spatial information, and can decode the output spike trains into recognizable inference results. Every neuron in the VFA decoding layer corresponds to a class, so the number of neurons in this layer is equal to the number of all possible classes in the target classification task. The spiking neuron model used in the VFA decoding layer is a specially designed voltage-based IF model whose threshold is set to be infinite, meaning this neuron has no ability to fire spikes, and its membrane voltage increases from 0 to infinity when it receives spikes. Actually, this neuron serves as a vote counter to accumulate the votes from the output neurons. The class corresponding to the neuron with the highest membrane voltage is the final inference result.

The VFA decoding layer only works during inference and is excluded during training. Therefore, its synaptic weights are fixed to be 0 during training. After the training is done, we calculate the synaptic weights of the VFA

decoding layer based on each output neuron's spiking response to training samples. We define w_{ij} as the synaptic weight between the i^{th} output neuron and the j^{th} neuron in the VFA decoding layer. The w_{ij} can be calculated as follows:

$$w_{ij} = \frac{s_{ij}^\mu}{\sum_{k=1}^C s_{ik}^\mu}, \quad (6)$$

where μ is an empirical constant, C is the number of the neurons in the VFA decoding layer, and s_{ij} represents the average number of the spikes fired by the i^{th} output neuron when a training sample belonging to the j^{th} class is input.

4.3 Adaptive Repolarization

To further accelerate the SNN's learning, we proposed to use adaptive repolarization in the output neurons, in which the winner neurons tend to fire more, thus accelerating the learning of the winner neurons, while other non-winner neurons tend to fire less. Here we define the winner neuron as the output neuron that is highly active to a certain training sample. The winner neuron is highly active because its represented feature is similar to this training sample. If we reinforce its spiking activity, the updates of its synaptic weights can be triggered more frequently, thus accelerating the learning. The adaptive repolarization is described as follows:

$$\psi = \begin{cases} v_{reset} + \alpha \Delta C & (\Delta g > 0) \\ v_{reset} - \alpha \Delta C & (\Delta g < 0) \\ v_{reset} & (\Delta g = 0) \end{cases}, \quad (7)$$

$$\Delta g = (g_e(t_f) - g_e(t_{f-1} + T_{ref})) - (g_i(t_f) - g_i(t_{f-1} + T_{ref})), \quad (8)$$

$$\Delta C = v_{thres} - v_{rest}, \quad (9)$$

where ψ is the adaptive resetting voltage (replacing the original fixed resetting voltage v_{reset}), t_f/t_{f-1} denote the time when this/last spike is fired, $g_{e/i}(t)$ is the value of $g_{e/i}$ at the time t , and α is a hyperparameter ranging from 0 to 1. As is shown in Fig. 4, the ψ increases by $\alpha \Delta C$ if the neuron gets more excitation than inhibition from $t_{f-1} + T_{ref}$ to t_f , and vice versa. Therefore, the spiking activities of winner neurons are enhanced, and other neurons are inhibited.

Theoretically, a larger α can accelerate the SNN's learning more, but it might let a few neurons fire excessive spikes and dominate the firing activity of the whole competition area. Therefore, there exists a tradeoff between learning efficiency and learning capability. To ease this problem, we set a large α at the beginning of the training, and then reduce the α as the training goes, which allows the SNN to converge quickly at the beginning but finally still achieve the same-level learning capability. This part will be further discussed in Section 7.3.

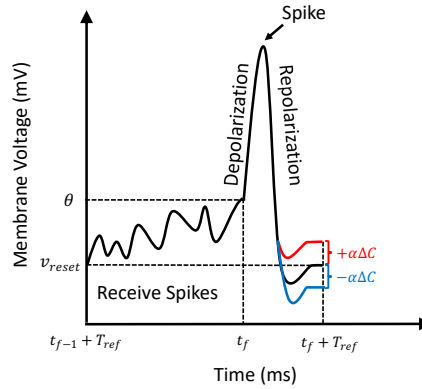


Fig. 4. An illustration of adaptive repolarization. The resetting voltage ψ is adaptive based on the spikes received from $t_{f-1} + T_{ref}$ to t_f .

5 Experimental Setup

5.1 Datasets

- MNIST [23]: The MNIST dataset contains 70,000 hand-written digit images (28×28 in size), split into 60,000 images for training and 10,000 images for testing. These images are labeled into 10 classes from 0 to 9.
- EMNIST [24]: This dataset is an extension of MNIST to hand-written English alphabet letters. There are six partitions in the EMNIST dataset, and we used the letter partition of them. The letter partition contains

145,600 hand-written letter images (28×28 in size), split into 124,800 images for training and 20,800 images for testing. These images are labeled into 26 classes corresponding to the 26 capital letters.

5.2 Baseline Methods

We evaluated our SNN in terms of learning capability (i.e. classification accuracy), learning efficiency, and robustness against hardware damage. We compared our method with the following baseline methods:

- Diehl-FC [7]: A 3-layer unsupervised FC SNN composed of conductance-based LIF models, and combined with the preliminary version of competitive learning (Fig. 2(a)) and triplet STDP. This work has been widely adopted as a baseline method [8-13]. The public code provided by [7] was used in the experiments for a fair comparison.
- Saunders-LC [8]: A 2-layer unsupervised LC SNN composed of current-based LIF models, and combined with the alternative version of competitive learning (Fig. 2(b)) and a simplified STDP. This work is the first one to adopt LC architecture in SNN. For a fair comparison, we strictly followed [8] to implement this method in the experiments, except that the size of its input layer was changed from 20×20 to 28×28.

The two baseline methods above are chosen because the three of us (i.e. Diehl-FC, Saunders-LC, and ours) all focus on the design of network architecture. Diehl-FC and Saunders-LC represent the widely used FC and LC architecture. Other unsupervised SNNs (e.g. [9-10]) aren't our opponents because they didn't focus on architecture and their contributions (e.g. learning theory, advanced STDP rule, etc.) can be utilized on our network architecture as well.

We also analyzed the effectiveness of our three contributions through some ablation studies. We evaluated the performance degradation when each contribution was removed or replaced by an existing method as follows:

- Ours-FC: Our Inception-like architecture is replaced by the FC architecture combined with the alternative version of competitive learning (Fig. 2(b)).
- Ours-LC: Our Inception-like architecture is replaced by the LC architecture combined with the alternative version of competitive learning (Fig. 2(b)).
- Ours-noVFA: The VFA decoding layer is replaced by the classic vote-based spike decoding scheme.
- Ours-noAR: The Adaptive Repolarization (AR) in the output neurons is removed, so the LIF model with a fixed resetting voltage v_{reset} is used as output neurons.

More details about the baseline methods are shown in Table 1.

5.3 Training Procedure

We used a training procedure similar to the one used in [7]: In each iteration, we present an image in the training set to the network for 350ms, and then there is a 150ms phase without any input to allow all variables of all neurons to decay to their default values. We train our SNN with a single pass through the training set, which leads to 60,000/124,800 training iterations in total (one image per iteration) for MNIST/EMNIST. After the training is done, we set the learning rate to zero and fix all synaptic weights. The synaptic weights of the VFA decoding layer are calculated based on the spiking responses of output neurons to the last 10,000 training images. Besides, we adopted the weight normalization scheme used in [8]: After each iteration, the sum of synaptic weights incident to an output neuron is normalized to be equal to c_{norm} (i.e. normalization constant). More implementation details including our code are presented in Appendix A1.

Table 1. Details of Baseline Methods

SNN	Architecture	Spike Decoding	Adaptive Repolarization	Competitive Learning	Neuron Model	STDP Model
Diehl-FC	FC	Classic vote-based decoding	no	Preliminary version (Fig. 2(a))	conductance-based LIF	Triplet STDP
Saunders-LC	LC	2-gram [8]	no	Alternative version (Fig. 2(b))	current-based LIF	Simplified typical STDP
Ours	Ours (Fig. 3)	VFA decoding layer	yes	Alternative version (Fig. 2(b))	conductance-based LIF	Triplet STDP
Ours-FC	FC	VFA decoding layer	yes	Alternative version (Fig. 2(b))	conductance-based LIF	Triplet STDP
Ours-LC	LC	VFA decoding layer	yes	Alternative version (Fig. 2(b))	conductance-based LIF	Triplet STDP
Ours-noVFA	Ours (Fig. 3)	Classic vote-based decoding	yes	Alternative version (Fig. 2(b))	conductance-based LIF	Triplet STDP
Ours-noAR	Ours (Fig. 3)	VFA decoding layer	no	Alternative version (Fig. 2(b))	conductance-based LIF	Triplet STDP

6 Evaluation

6.1 Learning Capability

In Table 2, we report the classification accuracy on the testing set of MNIST/EMNIST and the number of used neurons/synapses, $n_{neuron}/n_{synapse}$. Here we use $(k, s) \times F$ to denote the kernel size (k), stride (s), and feature map number (F) of a FC/LC architecture. As is mentioned in Section 4.1, each output neuron in FC architecture can be regarded as a feature map, and the (k, s) of a FC architecture is (28,1). In Table 2, our SNN achieves much improved testing results. Even more than 10% improvement on the EMNIST is achieved by our SNN. Besides, the networks with a larger size normally exhibit better testing results, while, compared with Diehl-FC and Saunders-LC, our SNNs can achieve higher testing results with fewer neurons and synapses used. Note that we didn't test our SNN with $Size_{SA} > 400$ because the SNNs with $Size_{SA} \leq 400$ have exhibited satisfactory results, but we anticipate that a larger $Size_{SA}$ will lead to a better result when computing resources are sufficient.

Table 3 shows the testing results of an ablation study where each contribution is removed respectively. The experimental results on the MNIST/EMNIST dataset show that: 1) Ours-FC and Ours-LC degrade in testing result, which further demonstrates that our proposed architecture outperforms the widely used FC/LC architecture on learning capability. 2) Our-noAR shows a slightly improved testing result. This means the adaptive repolarization only has a negligible impact on learning capability but can obviously improve the network's learning speed (shown in Section 6.2). 3) The testing result of Our-noVFA declines dramatically and is even lower than the one of Diehl-FC. This is because the classic vote-based decoding only works in FC architecture, while, in other architectures (e.g. LC, ours), it will cause a larger information loss in the spike decoding. Our architecture has superior learning capability, but this capability can't be reflected without the VFA decoding layer. This part will be further discussed in Section 7.2.

In Table 4, we compared our method with the various existing unsupervised SNN algorithms on the MNIST dataset. The results of compared algorithms are directly got from the corresponding references. Note that the semi-supervised algorithms (e.g. [27-30]) are excluded because they use extra supervised classifiers. Our method reaches a superior result than most of the compared algorithms. Panda et al. [9] and She et al. [10] achieve higher results through advanced learning rules (ASP, stochastic STDP), but they are still limited by slow-learning FC architecture. Our contributions are mainly on architecture design, so other SNN components (e.g. neuron model, learning rule and etc.) are very basic. Our architecture can be in conjunction with other more advanced SNN components to build a superior SNN algorithm.

Table 2. Comparison of Learning Capability

SNN	Topology	n_{neuron}	$n_{synapse}$	MNIST	EMNIST
Diehl-FC	$(28,1) \times 400$	800	473K	87.88%	66.41%
	$(28,1) \times 800$	1600	1267K	90.22%	67.45%
	$(28,1) \times 1600$	3200	3814K	91.96%	68.23%
	$(28,1) \times 6400$	12800	45977K	94.97%	47.41%*
Saunders-LC	$(16,6) \times 100$	900	320K	91.36%	62.37%
	$(16,6) \times 400$	3600	2361K	93.97%	66.78%
	$(16,6) \times 800$	7200	7603K	94.83%	68.83%
	$(16,6) \times 1000$	9000	11304K	95.02%	69.68%
Ours	$Size_{SA} = 100$	2100	1214K	93.16%	73.93%
	$Size_{SA} = 200$	4200	2849K	94.19%	76.45%
	$Size_{SA} = 300$	6300	4904K	94.95%	78.76%
	$Size_{SA} = 400$	8400	7379K	95.64%	80.11%

* The training is divergent, and the highest result before divergence is listed.

Table 3. Testing Results of Ablation Study

SNN	Topology	MNIST	EMNIST
Ours	$Size_{SA} = 400$	95.64%	80.11%
Ours-FC	$(28,1) \times 6400$	95.06%	56.16%*
Ours-LC	$(16,6) \times 1000$	95.26%	77.85%
Our-noAR	$Size_{SA} = 400$	95.67%	80.21%
Our-noVFA	$Size_{SA} = 400$	94.88%	69.27%

* The training is divergent, and the highest result before divergence is listed.

Table 4. Comparison of Testing Results on the MNIST Dataset among the Existing Unsupervised SNN Algorithms

Paper	Description	Result
Diehl et al. 2015 [7]	FC SNN (Diehl-FC)	95.00%
Saunders et al. 2019 [8]	LC SNN (Saunders-LC)	95.07%
Panda et al. 2017 [9]	FC SNN with Adaptive Synaptic Plasticity (ASP)	96.80%
She et al. 2019 [10]	FC SNN with stochastic STDP	96.10%
Rathi et al. 2018 [11]	Sparsely connected SNN with STDP-based connection pruning	90.10%
Lammie et al. 2018 [12]	FPGA neuromorphic system based on FC SNN	94.00%
Allred et al. 2016 [13]	FC SNN using forced firing of dormant or idle neurons	85.90%
Querlioz et al. 2011 [14]	Memristor-Based SNN	93.50%
Ours	High-parallelism Inception-like SNN	95.64%

6.2 Learning Efficiency

In Fig. 5, we report the MNIST testing results of the networks trained with varying number of training iterations. In Fig. 5(a), we compare the SNNs with similar learning capability: Diehl-FC with $(28,1) \times 6400$, Saunders-LC with $(16,6) \times 800$, and our SNN with $Size_{SA} = 300$. These three SNNs all exhibit close learning capabilities of about 94.9% results when fully trained. It's shown in Fig. 5(a) that our SNN exhibits much superior learning efficiency. The testing results of our SNN can achieve nearly 80%, 90% accuracy after the training with only 500, 2500 iterations, while Saunders-LC just achieves nearly 30%, 75% accuracy with 500, 2500 training iterations, and worst of all, Diehl-FC only reaches nearly 42% accuracy with even 10,000 training iterations. Note that Saunders-LC and our SNN can be fully trained within one pass through the training set, but Diehl-FC needs to be trained with 15 passes through the training set, leading to 900,000 training iterations in total.

Fig. 5(b) shows the results of an ablation study where Ours-FC with $(28,1) \times 6400$, Ours-LC with $(16,6) \times 800$, and Ours/Ours-noVFA/Ours-noAR with $Size_{SA} = 300$ are tested for learning efficiency. The experimental results show that: 1) Ours-FC and Ours-LC show much slower learning speed than our original SNN, which demonstrates that our proposed architecture also outperforms the FC/LC architecture on learning efficiency. 2) The learning efficiency of Ours-noAR also degrades, meaning that the adaptive repolarization indeed accelerates our SNN's learning. 3) The testing curve of Ours-noVFA is below the one of our original SNN, but they have a similar growing pace, which means that the VFA decoding layer improves the network's inference accuracy but doesn't have an obvious impact on the network's learning efficiency.

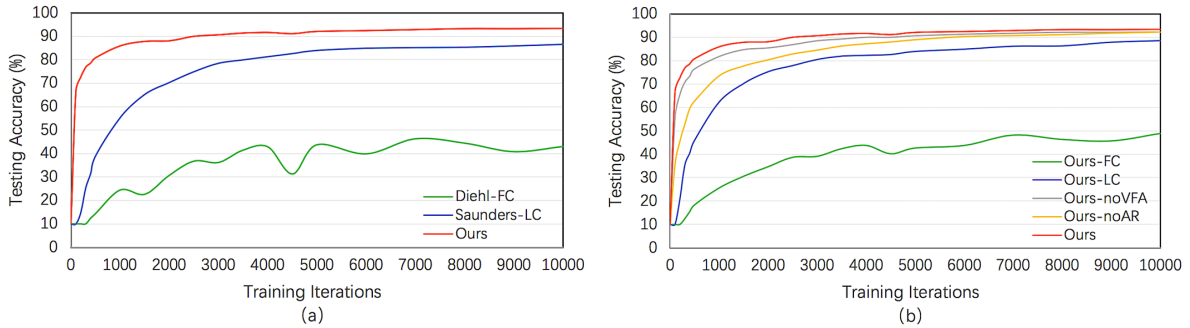


Fig. 5. Testing results of the SNNs trained with varying number of training iterations. (a) Comparison among Diehl-FC, Saunders-LC, and ours. (b) Ablation study.

6.3 Robustness

Robustness means the SNN's resistance against hardware damage and destruction. To evaluate it, we followed the experiment used in [8]. This experiment simulates a situation when SNN-based hardware gets physical damage or even destructed. Concretely, we randomly deleted the output neurons or learnable synapses of trained SNNs with probability ρ_{delete} , then report their testing results on the MNIST dataset in Fig. 6.

Fig. 6(a)/(b) shows the robustness testing results of Diehl-FC with $(28,1) \times 6400$, Saunders-LC with $(16,6) \times 800$, and our SNN with $Size_{SA} = 300$. The three SNNs without any neuron/synapse deletion have similar learning capability, all reaching a result of about 94.9%, while deleting neuron/synapse leads to performance degradation. Fig. 6(a) shows the testing results after deleting neurons with probability ρ_{delete} and our SNN exhibits the highest

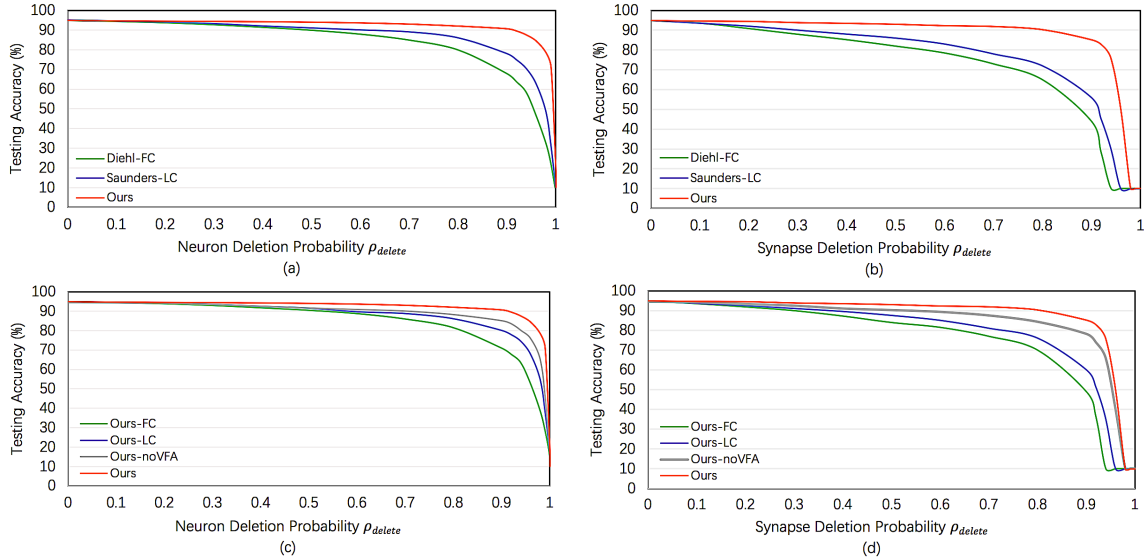


Fig. 6. Testing results of the SNNs whose neurons/synapses are randomly deleted with varying probability p_{delete} . (a) Neuron deletion. (b) Synapse deletion. (c)/(d) Ablation studies for neuron/synapse deletion.

robustness: Our SNN achieves nearly 90%, 80% results even if 90%, 95% of neurons are deleted, while Diehl-FC and Saunders-LC achieve nearly 80% and 85% results respectively with only 80% of neurons deleted. Similarly, Fig. 6(b) shows the testing results after deleting synapses with probability p_{delete} and our SNN still exhibits the highest robustness: Our SNN achieves nearly 90%, 80% results even if 80%, 90% of synapses are deleted, while Diehl-FC and Saunders-LC just achieve nearly 70% and 65% results with only 80% of synapses deleted. This experiment demonstrate that our SNN has higher robustness against hardware damage. It can work well even when most of its learnable synapses or computing neurons have broken down.

Also, we tested Ours-FC with $(28,1) \times 6400$, Ours-LC with $(16,6) \times 800$, and Ours/Ours-noVFA with $Size_{SA} = 300$ in Fig. 6(c)/(d). The experimental results show that: 1) Ours-FC and Ours-LC show much degraded robustness compared with our original SNN, which demonstrates that our proposed architecture outperforms the FC/LC architecture on robustness. 2) Surprisingly, Ours-noVFA also shows degraded robustness, especially in Fig. 6(c) (neuron deletion), meaning that the VFA decoding layer helps improving the 's robustness. This is an unintended benefit because the VFA decoding layer was originally designed to reduce the information loss in the spike decoding and improve inference accuracy. The possible explanation for this will be discussed in Section 7.2. Note that the curve of Ours-noAR is not drawn in Fig. 6(c)/(d), because the adaptive repolarization only has a negligible impact on the SNN's robustness, and the curve of Ours-noAR is almost the same as the one of our original SNN.

7 Discussion

In Section 7.1, we analyze the parallelism of FC, LC, and our architectures. Our architecture consists of 21 sub-networks that can learn and compute in parallel, which explains our SNN's improved learning efficiency and robustness. In Section 7.2, the information loss in the spike decoding is analyzed. Our VFA decoding layer matches the learning nature of our architecture and results in less information loss. In Section 7.3, we discuss the relationship between spiking intensity and learning efficiency. The spiking intensity is tested to demonstrate that the adaptive repolarization can enhance the spiking activities of winner neurons, and thus accelerates learning.

7.1 Architecture Parallelism

A SNN's learning efficiency and robustness against hardware damage is highly relevant to its architecture parallelism. We assumed that, if a SNN consists of multiple independent sub-networks and these sub-networks can compute in parallel, this SNN can exhibit superior learning efficiency and robustness, because all sub-networks can learn simultaneously, and each sub-network can work well independently when other sub-networks get damaged or even destructed.

In competitive learning, as we mentioned in Section 3.5, a competition area is defined as a set of output neurons sharing the same RF, and each output neuron only competes with other neurons in the same competition area. According to this principle, a competition area can be regarded as a sub-network, because there is no interaction between two competition areas and each competition area can compute independently. Fig. 7 shows the partitions of

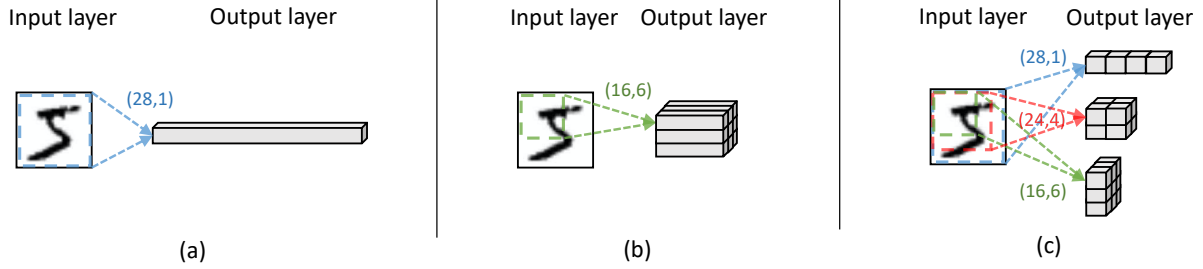


Fig. 7. An illustration of SNN’s competition areas. (a) FC architecture contains only a single competition area. (b) LC architecture contains 9 competition areas. (c) Our architecture contains 21 competition areas. Note that a cube denotes a competition area here.

the SNN’s competition areas (sub-networks). The widely used FC architecture has only a single competition area because all output neurons share the same global RF (see Fig. 7(a)). A large number of output neurons is located in one competition area, leading to sub-optimal learning efficiency and robustness. LC architecture eases this limitation by localizing the RF (see Fig. 7(b)), which allows the LC architecture to have multiple competition areas (sub-networks). Therefore, the LC architecture can exhibit improved learning efficiency and robustness. We took a further step based on the LC architecture: 1) Inspired by the Inception module in the ANN literature, we designed an Inception-like multi-pathway architecture to integrate multi-scale spatial information and improve the network’s parallelism. 2) We partitioned the original competition area into multiple sub-areas to further increase the number of competition areas. As is shown in Fig. 7(c), our architecture has 21 competition areas (sub-networks) in total, which explains why our architecture can outperform the FC/LC architecture in terms of learning efficiency and robustness.

7.2 Information Loss in the Spike Decoding

In the experiments, we found that the classic vote-based decoding scheme (denote by VFO here) works well in the FC architecture but performs badly in the LC and our architecture. We think this is because one underlying assumption of VFO is violated. The VFO assigns each output neuron to a certain class, and build a Vote-for-One (VFO) relationship between each output neuron and a certain class. Under this strategy, each output neuron can only vote for one certain class. This approach actually is based on an assumption that each output neuron is only highly responsive to one certain class. This assumption is feasible in the FC architecture because each output neuron can receive global information (see Fig. 8(a)). However, this assumption is violated in the LC architecture because the output neurons in this architecture can only receive local information (see Fig. 8(b)). Since the images belonging to different classes might have similar local features, theoretically an output neuron in the LC architecture can be highly responsive to more than one class. E.g., as can be seen in Fig. 8(b), the local features of digits ‘2’ and ‘3’ in the red square are quite similar to each other, so the output neurons corresponding to these RFs might be highly responsive to both ‘2’ and ‘3’ because they can’t classify ‘2’ and ‘3’ only based on the local feature. Violating this underlying assumption leads to a large information loss in the spike decoding. Similarly, the VFO is unsuitable for our architecture due to the same reason. In contrast to the VFO, the proposed VFA decoding layer (denoted by VFA here) builds a Vote-for-All (VFA) relationship between each output neuron and all possible classes, and thus allows each output neuron to vote for all classes, which greatly reduces the information loss in the spike decoding.

To validate our above hypothesis, in Fig. 9, we compared the performance improvements got by replacing VFO with VFA in three network architectures (FC with $(28,1) \times 6400$, LC with $(16,6) \times 1000$, and Ours with $Size_{SA} =$

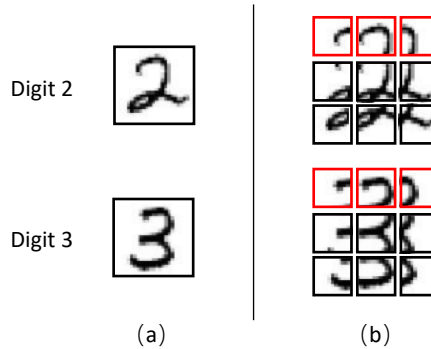


Fig. 8. Examples of output neuron’s RF in the (a) FC and (b) LC architecture when the input image is digit 2/3. The output neurons in (a) can see the whole input image, while the ones in (b) only can see a part of the input image.

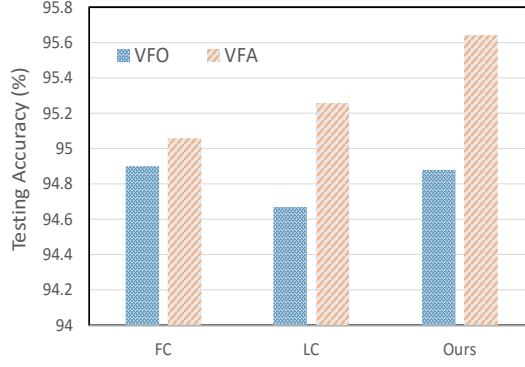


Fig. 9. The improvements in testing results got by replacing VFO with VFA in the FC/LC/Our architecture.

400) on the MNIST. For a fair comparison, these three architectures are implemented with the same LIF model, STDP rule, and alternative version (Fig. 2(b)) of competitive learning described in Section 3. The adaptive repolarization is not used here. The experimental results show that the LC and our architecture can gain more performance improvement than the FC architecture. This also demonstrates that, without VFA, LC and our architecture can't fully show its superior learning capability. We guess previous scholars might have tried to adopt Inception-like architecture as well, but they failed to get improvement without VFA.

Moreover, in Fig.6(c)/(d), we surprisingly found that the VFA decoding layer helps improving the network's robustness. The possible explanation is that, under the VFO approach, each class can only get votes from the output neurons assigned to this class, while, under the VFA approach, each class can get votes from all output neurons. In the latter case, even many broken neurons won't have a fatal impact on the final inference result because the remaining output neurons still can work together to conduct a reliable inference.

7.3 Spiking Intensity and Learning Efficiency

Theoretically, the learning efficiency of a STDP-based network is highly relevant to its spiking intensity, because, according to the STDP rule, the update of synaptic weight (i.e. learning) occurs when the pre/postsynaptic neuron fires a spike. To validate this hypothesis, we tested the average spiking intensity of Diehl-FC with $(28,1) \times 6400$, Saunders-LC with $(16,6) \times 1000$ and our SNN with $Size_{SA} = 400$, and report the results in Table 5. The experimental results show that the Saunders-LC and our SNN have higher spiking intensity than Diehl-FC, and ours has the highest spiking intensity. These results conform to the hypothesis that the SNN with higher spiking intensity exhibits faster learning speed. This also allows us to explain why our SNN can learn faster from another point of view.

The effect of adaptive repolarization on learning capability and learning efficiency is shown in Fig. 10, where we tested the average spiking intensity of our SNN with varying α of adaptive repolarization on the MNIST dataset. Note

Table 5. Comparison of Average Spiking Intensity

SNN	Spiking Intensity (spikes/iteration)
Diehl-FC	7.84
Saunders -LC	58.26
Ours	154.63

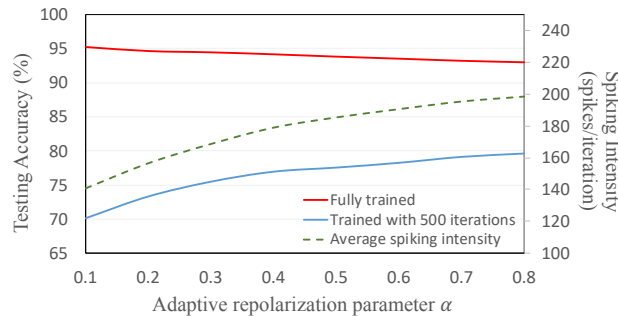


Fig. 10. Testing results and average spiking intensity of our SNN with varying α of adaptive repolarization.

that, in this experiment, the $Size_{SA}$ is set to be 400, and the α is fixed once it's set at the beginning of the training. Here we use the testing result of the SNN trained with 500 iterations to represent the learning efficiency, and use the testing result of the fully trained SNN to represent the learning capability. As is shown in Fig. 10, there is a trade-off between learning capability and learning efficiency: A larger α leads to higher spiking intensity and higher learning efficiency but lower learning capability. This experiment further shows the relationship between learning efficiency and spiking intensity, and also explains why we used a declined α in our final training procedure. Note that, as we mentioned in Section 4.3, the adaptive repolarization can enhance the spiking activities of winner neurons and hinder the ones of non-winner neurons. However, since the SNN's spiking intensity is dominated by winner neurons, we can only observe an increase of spiking intensity when the adaptive repolarization is used.

8 Conclusion and Future Work

In this paper, we proposed a fast-learning and high-robustness unsupervised SNN with a high-parallelism Inception-like network architecture. Our architecture outperforms the widely used FC and LC architecture, and our SNN achieves improvements in both the learning capability and learning speed, and it was shown to be robust against hardware damage. Moreover, the proposed VFA decoding layer was proved to be effective in reducing the information loss of spike decoding in the LC and our architectures.

Our method can be further improved. To emphasize the effectiveness of our contributions, other SNN components we used are very simple. We suggest that advanced SNN components (e.g. ASP [9], stochastic STDP [10], etc.) can be used to achieve better performance. Besides, although we used our Inception-like architecture on unsupervised SNNs, there is a possibility of it being added to supervised SNNs because our architecture can integrate multi-scale information (feature), which is helpful for supervised feature learning as well.

Appendix

A.1 Implementation details

Our experiments ran on an Ubuntu system with Python 2.7. Our code is based on an open-source simulator, Brian [37], and is available at <https://github.com/MungoMeng/Spiking-Inception>.

All hyperparameters used in our experiments are empirical values (in Table 6). The α of adaptive repolarization is 0.6 initially, and then halves every 5000 iterations. Finally, the α is set to 0 after the 20,000th iteration. We decided the hyperparameters through cross-validation, in which we randomly picked up 10,000/20,800 images from the training set of MNIST/EMNIST as the validation set.

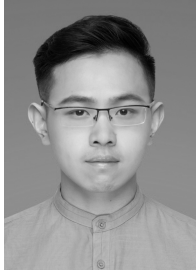
Table 6. Hyperparameter Settings in the Experiments

Hyperparameter	Description	Value
η_{post}	Postsynaptic learning rate	0.01
η_{pre}	Presynaptic learning rate	0.0001
τ_{pre}	Time constant of x_{pre}	20ms
$\tau_{post1}/\tau_{post2}$	Time constant of x_{post1}/x_{post2}	20ms/40ms
v_{thres}	Threshold voltage	-52mv
v_{rest}	Resting voltage	-65mv
v_{reset}	Reset voltage	-65mv
v_{exc}/v_{inh}	Equilibrium voltage	0mv/-100mv
θ_{plus}	Increment for adaptive threshold	0.05mv
T_{ref}	Time length of refractory period	5ms
τ_v	Time constant of v	100ms
τ_θ	Time constant of adaptive θ	10^7 ms
τ_{g_e}/τ_{g_i}	Time constant of g_e/g_i	1ms/2ms
c_{norm}	Weight normalization constant	78.4
μ	VFA decoding layer constant	0.1

References

- [1] O'reilly, Randall C., and Yuko Munakata. Computational explorations in cognitive neuroscience: Understanding the mind by simulating the brain. MIT press, 2000.
- [2] Tavanaei, Amirhossein, et al. "Deep learning in spiking neural networks." Neural Networks 111 (2019): 47-63.

- [3] Wade, John J., et al. "SWAT: a spiking neural network training algorithm for classification problems." *IEEE Transactions on Neural Networks* 21.11 (2010): 1817-1830.
- [4] Ponulak, Filip, and Andrzej Kasiński. "Supervised learning in spiking neural networks with ReSuMe: sequence learning, classification, and spike shifting." *Neural computation* 22.2 (2010): 467-510.
- [5] Xie, Xiurui, et al. "Efficient training of supervised spiking neural network via accurate synaptic-efficiency adjustment method." *IEEE transactions on neural networks and learning systems* 28.6 (2016): 1411-1424.
- [6] McKennoch, Sam, Dingding Liu, and Linda G. Bushnell. "Fast modifications of the spikeprop algorithm." *The 2006 IEEE International Joint Conference on Neural Network Proceedings*. IEEE, 2006.
- [7] Diehl, Peter U., and Matthew Cook. "Unsupervised learning of digit recognition using spike-timing-dependent plasticity." *Frontiers in computational neuroscience* 9 (2015): 99.
- [8] Saunders, Daniel J., et al. "Locally connected spiking neural networks for unsupervised feature learning." *Neural Networks* 119 (2019): 332-340.
- [9] Panda, Priyadarshini, et al. "Asp: Learning to forget with adaptive synaptic plasticity in spiking neural networks." *IEEE Journal on Emerging and Selected Topics in Circuits and Systems* 8.1 (2017): 51-64.
- [10] She, Xueyuan, Yun Long, and Saibal Mukhopadhyay. "Fast and Low-Precision Learning in GPU-Accelerated Spiking Neural Network." *2019 Design, Automation & Test in Europe Conference & Exhibition (DATE)*. IEEE, 2019.
- [11] Rathi, Nitin, Priyadarshini Panda, and Kaushik Roy. "STDP-based pruning of connections and weight quantization in spiking neural networks for energy-efficient recognition." *IEEE Transactions on Computer-Aided Design of Integrated Circuits and Systems* 38.4 (2018): 668-677.
- [12] Lammie, Corey, Tara Hamilton, and Mostafa Rahimi Azghadi. "Unsupervised character recognition with a simplified fpga neuromorphic system." *2018 IEEE International Symposium on Circuits and Systems (ISCAS)*. IEEE, 2018.
- [13] Allred, Jason M., and Kaushik Roy. "Unsupervised incremental stdp learning using forced firing of dormant or idle neurons." *2016 International Joint Conference on Neural Networks (IJCNN)*. IEEE, 2016.
- [14] Querlioz, Damien, Olivier Bichler, and Christian Gamrat. "Simulation of a memristor-based spiking neural network immune to device variations." *The 2011 International Joint Conference on Neural Networks*. IEEE, 2011.
- [15] Xing, Fu, et al. "Homeostasis-Based CNN-to-SNN Conversion of Inception and Residual Architectures." *International Conference on Neural Information Processing*. Springer, Cham, 2019.
- [16] Neil, Daniel, Michael Pfeiffer, and Shih-Chii Liu. "Learning to be efficient: Algorithms for training low-latency, low-compute deep spiking neural networks." *Proceedings of the 31st annual ACM symposium on applied computing*. 2016.
- [17] Rueckauer, Bodo, et al. "Conversion of continuous-valued deep networks to efficient event-driven networks for image classification." *Frontiers in neuroscience* 11 (2017): 682.
- [18] Cao, Yongqiang, Yang Chen, and Deepak Khosla. "Spiking deep convolutional neural networks for energy-efficient object recognition." *International Journal of Computer Vision* 113.1 (2015): 54-66.
- [19] K. He, X. Zhang, S. Ren, and J. Sun, "Delving deep into rectifiers: Surpassing human-level performance on ImageNet classification," in *Proc. IEEE Int. Conf. Comput. Vis.*, Dec. 2015, pp. 1026-1034.
- [20] D. Silver et al., "Mastering the game of go with deep neural networks and tree search," *Nature*, vol. 529, no. 7587, pp. 484-489, 2016.
- [21] Y. LeCun, Y. Bengio, and G. Hinton, "Deep learning," *Nature*, vol. 521, pp. 436-444, May 2015.
- [22] Szegedy, Christian, et al. "Going deeper with convolutions." *Proceedings of the IEEE conference on computer vision and pattern recognition*. 2015.
- [23] LeCun, Yann, Corinna Cortes, and C. J. Burges. "Mnist handwritten digit database. AT&T Labs." (2010).
- [24] Cohen, Gregory, et al. "EMNIST: Extending MNIST to handwritten letters." *2017 International Joint Conference on Neural Networks (IJCNN)*. IEEE, 2017.
- [25] Szegedy, Christian, et al. "Rethinking the inception architecture for computer vision." *Proceedings of the IEEE conference on computer vision and pattern recognition*. 2016.
- [26] Szegedy, Christian, et al. "Inception-v4, inception-resnet and the impact of residual connections on learning." *Thirty-First AAAI Conference on Artificial Intelligence*. 2017.
- [27] Kheradpisheh, Saeed Reza, et al. "STDP-based spiking deep convolutional neural networks for object recognition." *Neural Networks* 99 (2018): 56-67.
- [28] P. Falez, P. Tirilly, I. Marius Bilasco, P. Devienne and P. Boulet, "Multi-layered Spiking Neural Network with Target Timestamp Threshold Adaptation and STDP," *2019 International Joint Conference on Neural Networks (IJCNN)*, Budapest, Hungary, 2019, pp. 1-8.
- [29] Tavanaei, Amirhossein, and Anthony S. Maida. "Multi-layer unsupervised learning in a spiking convolutional neural network." *2017 International Joint Conference on Neural Networks (IJCNN)*. IEEE, 2017.
- [30] Lee, Chankyu, et al. "Deep spiking convolutional neural network trained with unsupervised spike-timing-dependent plasticity." *IEEE Transactions on Cognitive and Developmental Systems* 11.3 (2018): 384-394.
- [31] Hodgkin, Alan L., and Andrew F. Huxley. "A quantitative description of membrane current and its application to conduction and excitation in nerve." *The Journal of physiology* 117.4 (1952): 500-544.
- [32] Izhikevich, Eugene M. "Simple model of spiking neurons." *IEEE Transactions on neural networks* 14.6 (2003): 1569-1572.
- [33] Gerstner, Wulfram, et al. *Neuronal dynamics: From single neurons to networks and models of cognition*. Cambridge University Press, 2014.
- [34] Bichler, Olivier, et al. "Unsupervised features extraction from asynchronous silicon retina through spike-timing-dependent plasticity."
- [35] Pfister, Jean-Pascal, and Wulfram Gerstner. "Triplets of spikes in a model of spike timing-dependent plasticity." *Journal of Neuroscience* 26.38 (2006): 9673-9682.
- [36] Morrison, Abigail, Ad Aertsen, and Markus Diesmann. "Spike-timing-dependent plasticity in balanced random networks." *Neural computation* 19.6 (2007): 1437-1467.
- [37] Goodman, Dan FM, and Romain Brette. "The brian simulator." *Frontiers in neuroscience* 3 (2009): 26.
- [38] Meng, Mingyuan, et al. "Spiking Inception Module for Multi-layer Unsupervised Spiking Neural Networks." *arXiv preprint arXiv:2001.10696* (2020). (Accepted at the IJCNN2020)
- [39] Meng, Mingyuan, et al. "High-parallelism Inception-like Spiking Neural Networks for Unsupervised Feature Learning" *arXiv preprint arXiv:2001.01680* (2019).



Mingyuan Meng received the B.E. degree in electronic information science and technology from Tsinghua University, Beijing, China, in 2018. He is currently pursuing a Ph.D. degree with the School of Computer Science, the University of Sydney, Sydney, Australia.

He was a research assistant at the School of Electronics and Information Technology, Sun Yat-Sen University, Guangzhou, China, in 2019. His current research interests include machine learning, artificial/spiking neural networks, and corresponding medical applications.



Xingyu Yang is currently pursuing the graduate degree with the School of Electronic Information and Engineering, Sun Yat-Sen University of China, Guangzhou, China, from 2019. Her current research interests include spiking neural networks, spiking neuron models, and neuromorphic hardware.



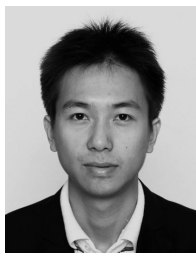
Lei Bi received his master of information technology, master of philosophy (research) and PhD from the University of Sydney, in 2011, 2013 and 2018, respectively.

Currently, he is a research fellow with the Australia Research Council Training Centre in Innovative BioEngineering, the University of Sydney. His research interests include in using deep learning technologies for computer-aided diagnosis and medical image analysis.



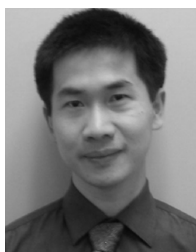
Jinman Kim received the B.S. (honours) degree in computer science and PhD degree from the University of Sydney, Australia, in 2001 and 2006, respectively.

Since his PhD, he has been a Research Associate at the leading teaching hospital, the Royal Prince Alfred. In 2008 until 2012, he was an ARC postdoc research fellow, one year leave (2009-2010) to join MIRALab research group, Geneva, Switzerland, as a Marie Curie senior research fellow. Since 2013, he has been with the School of Computer Science, The University of Sydney, where he was a Senior Lecturer, and became an Associate Professor in 2016. His research interests include medical image analysis and visualization, computer aided diagnosis, and Telehealth technologies.



Shanlin Xiao received the B.S. degree in communications engineering and the M.S. degree in communications and information systems from the University of Electronic Science and Technology of China (UESTC), Chengdu, China, in 2009 and 2012, respectively. He received his Ph.D. degree in Communications and Computer Engineering from the Tokyo Institute of Technology, Tokyo, Japan, in 2017.

He is currently an associate research professor at the School of Electronics and Information Technology in Sun Yat-Sen University, Guangzhou, China. His research interests include domain-specific architecture for artificial intelligence and neuromorphic computing.



Zhiyi Yu received the B.S. and M.S. degrees in EE from Fudan University, China, in 2000 and 2003, respectively, and the Ph.D. degree in ECE from the University of California at Davis, CA, USA, in 2007.

He was with IntellaSys Corporation, CA, USA, from 2007 to 2008. From 2009 to 2014, he was an associate professor in the Department of Microelectronics, Fudan University, China. Currently, he is a professor at the school of electronics and information technology, Sun Yat-sen University, China. His research interests include digital VLSI design and computer architecture. Dr. Yu serves as TPC member on many conference committees, such as the ASSCC, VLSI-SOC, ISLPED, APSIPA, SASIM.